Published in final edited form as:
NMR Biomed. 2013 September ; 26(9): 1142–1151. doi:10.1002/nbm.2928.

Three dimensional mapping of the creatine kinase enzyme reaction rate in muscles of the lower leg

Prodromos Parasoglou[1,*], **Ding Xia**[1], **Gregory Chang**[1], **Antonio Convit**[2], and **Ravinder R. Regatte**[1]

[1]Quantitative Multinuclear Musculoskeletal Imaging Group (QMMIG), Department of Radiology, Center for Biomedical Imaging, New York University Langone Medical Center, New York, NY, USA

[2]Departments of Psychiatry and Medicine, New York University Langone Medical Center, New York, NY, USA

Abstract

Phosphorous (^{31}P) magnetization transfer (MT) techniques enable the non-invasive measurement of metabolic turnover rates of important enzyme catalyzed reactions, such as the creatine kinase reaction (CK), a major transducing reaction involving adenosine triphosphate and phosphocreatine. Alteration in the kinetics of the CK reaction rate appears to play a central role in many disease states.

In this study, we developed and implemented at ultra-high field (7T), a novel three-dimensional ^{31}P-MT imaging sequence that maps the kinetics of CK in the entire volume of the lower leg at relatively high resolution (0.52 mL voxel size), and within acquisition times that can be tolerated by patients (below 60 min). We tested the sequence on five healthy and two clinically diagnosed type 2-diabetic patients. Overall, we obtained measurements that are in close agreement with measurements reported previously using spectroscopic methods. Importantly, our spatially resolved method allowed us to measure local CK reaction rate constants and metabolic fluxes in individual muscles in healthy subjects. Furthermore, in the case of patients with diabetes, it allowed us to detect variations of the CK rate of different muscles, which would not have been possible using unlocalized MRS methods.

The results of this work suggest that 3D-mapping of the CK reaction rates and metabolic fluxes can be achieved in the skeletal muscle *in* vivo at relatively high spatial resolution and with acquisition times well tolerated by patients. The ability to measure bioenergetics simultaneously in large areas of muscles will bring new insights into possible heterogeneous patterns of muscle metabolism associated with several diseases and serve as a valuable tool for monitoring the efficacy of interventions.

Keywords

Magnetization Transfer; Phosphorus MRI; Muscle Metabolism; Creatine Kinase

[*]Correspondence to: Prodromos Parasoglou, PhD, Center of Biomedical Imaging, Department of Radiology, NYU Langone Medical Center, 660 First Avenue (4th floor), New York, NY 10016. Tel: +1-212-263-2700, Fax: +1-212-263-7541, prodromos.parasoglou@nyumc.org.

Introduction

Phosphorus Magnetic Resonance Spectroscopy (^{31}P-MRS) has been established as the standard non-invasive technique for studying bioenergetics in the human skeletal muscle (1). Besides providing measurement of the concentration of several key metabolites, ^{31}P-MRS also allows the assessment of metabolic turnover rates in resting muscles by means of magnetization transfer (MT) methods (2). Tissues with high energy demand (such as the skeletal muscle, heart or brain), buffer against adenosine triphosphate (ATP) depletion via a reservoir of energy in the form of phosphocreatine (PCr), which is utilized by the creatine kinase (CK) enzyme reaction to recycle adenosine diphosphate (ADP) rapidly back to ATP (3). Alteration in the kinetics of the CK reaction rate appear to play a central role in many disease states, including ischemic heart disease (4), heart failure (5), stroke and congenital myopathies (6), inflammatory myopathies (7), type 2 diabetes (8,9) and peripheral arterial disease (10).

Phosphorus containing metabolite concentrations in skeletal muscle are in the millimolar range, which combined with the low gyromagnetic ratio (γ) of the ^{31}P nucleus result in low MR sensitivity and require long acquisition times when compared to ^{1}H-MR. Therefore, most of the previous ^{31}P-MRS studies have employed small surface radiofrequency (RF) coils and used either unlocalized or gradient-localized single voxel pulse-acquire sequences by taking measurements from large areas of tissue (11). However, with this approach the measured MR signals often represent weighted averages originating from heterogeneous structures (12). In addition, the profile sensitivity of surface coils mostly allows measurements from superficial tissues. Normal aging (13) and several diseases are known to result in heterogeneous patterns of altered metabolic function (14) that cannot be captured by single-voxel techniques, and therefore the need to develop new imaging methods to study inhomogeneous patterns of disease progression and follow intervention efficacies longitudinally (15).

Magnetization transfer techniques are inherently time consuming because they require multiple experiments, including spin-lattice (T_1) relaxation measurements. Most of the ^{31}P containing metabolites are characterized by very long T_1s (~2–7 s) (16), and therefore the experiment is very inefficient in delivering signal-to-noise ratio (SNR) per unit time. Therefore, in vivo ^{31}P-MT spectroscopic imaging experiments suffer from long acquisition times that cannot be easily tolerated by patients. Several studies have shown the feasibility of performing MT spectroscopic imaging in the brain at coarse resolution (~ 6–8 mL voxel size) (17,18). However, despite the fact that faster ^{31}P-MRS techniques have been proposed in the literature (19,20), we are not aware of previous efforts to measure metabolic fluxes in skeletal muscle with 3D-volumetric coverage.

Compared to spectroscopic imaging methods, spectrally selective imaging pulse sequences that measure one ^{31}P containing metabolite are inherently more time efficient (21–25), and have been used to measure both baseline concentrations and dynamic changes of one metabolite (i.e. PCr) following physical exercise (26). In our previous work (27), we have demonstrated that three-dimensional mapping of PCr concentration in several muscles of the lower leg is feasible both at high (3T) and ultra-high (7T) field strength at significantly improved spatial resolution (0.52 mL nominal voxel size) using a 3D-turbo spin echo sequence compared to conventional ^{31}P-MRS. At relatively lower spatial resolution (1.6 mL at 7T, and 4.2 mL 3T) we also showed that 3D-mapping of the dynamics of PCr resynthesis following exercise can also be achieved with a temporal resolution between 12 to 24 s (28,29).

In the current work, we are focusing on the development and implementation of a 3D-MT imaging method at ultra high field which allows mapping of the metabolic fluxes of the CK reaction rate in several muscles of the lower leg, at relatively high spatial resolution (0.52 mL), while maintaining the total acquisition time at levels that can be tolerated by patients (below 60 min).

Theory

A unique feature of magnetic resonance is that under certain conditions the measured signal can provide quantitative information about the rate of metabolic turnover even under steady state conditions in the absence of any net changes in metabolite levels (11). Transfer of magnetization between γ-ATP, PCr and Pi that are linked by chemical exchange can be studied by selective perturbation of the equilibrium magnetization of one of the nuclei that is involved in the exchange process and measuring the effect on the signal from its exchange partner (30). More specifically, in the case of the CK reaction, the MT experiment is used to estimate the pseudo-first order rate of the phosphorus exchange between PCr and γ-ATP.

$$PCr + \text{adenosine diphosphate}\,(ADP) + H^{+} \leftrightarrow ATP + \text{creatine}$$

Estimation of the pseudo-first order rate of exchange, k_{CK} (forward direction), requires measurement of the PCr signal when the magnetization of γ-ATP is perturbed (M_z), in addition to a control experiment when the mirrored side of the PCr is irradiated (M_0), together with the measurement of the spin-lattice relaxation time (T_1') of PCr measured with the γ-ATP saturated (2). The forward CK reaction rate is then calculated using the following equation:

$$k_{CK} = \left(\frac{1 - M_z/M_0}{T_1'} \right) \quad [1]$$

The metabolic flux of the reaction (V_{CK}) is calculated from the product of the pseudo-first order rate constant and the PCr concentration:

$$V_{CK} = k_{CK} \cdot [\mathrm{PCr}] \quad [2]$$

Materials and Methods

Human Subjects

We recruited five healthy volunteers (three male and two female, 30.4 ± 4.0 years of age, with BMI < 26.0), and two clinically diagnosed type 2-diabetic patients. The patient characteristics were respectively: age (48 and 58), sex (both male), BMI (26.2 and 34.1 kg/m^2), fasting glucose (134 and 194 mg/dl), fasting insulin (19 and 15 mIU/mL), HOMA-IR (6.22 and 7.13) and HbA1c (11.6 and 9.7%). In addition, both patients with diabetes, given their poor glucose control, were on both metformin and insulin treatment, as well as on antihypertensive and cholesterol lowering drugs. Both participants with diabetes had normal kidney function parameters. All subjects were scanned on a 7T MRI system (Siemens Medical Solutions, Erlangen, Germany) using a dual-tuned $^{31}P/^{1}H$ quadrature transmit-receive knee coil (Rapid MRI, Ohio) with 18 cm inner diameter and 20 cm length. The New York University School of Medicine Institutional Review Board approved the study, and all subjects provided informed written consent for participation in the study.

^{31}P-MRS

At the beginning of all measurement sessions, we used an iterative first and second order-shimming algorithm (provided by the manufacturer) on the entire volume of the calf muscle, which typically resulted in PCr peak linewidth of 24 ± 8 Hz, while the linewidth of the water peak was 75 ± 10 Hz.

Continuous wave (CW) RF irradiation enables effective saturation. However, high RF energy deposition in tissue (defined as the specific absorption rate SAR), as well as limited pulse width and duty cycle, limit the application of CW irradiation in clinical MR scanners. To overcome these constraints, frequency selective trains of pulses may be used (31). In our study, we employed a train of frequency selective Gaussian pulses of 100 ms duration each.

In order to define the total irradiation time (i.e. number of Gaussian pulses), to be used in the MT-imaging experiment and the power of the pulses (denoted here as the nominal flip angle) pulse optimization was performed on two healthy volunteers using an unlocalized product pulse acquire sequence with 15 s repetition time, TR, which acquired 2048 complex points of the free induction decay with a spectral width of 5000 Hz, and four averages. The area under the PCr peak of the control (irradiation at +2.48 ppm) and irradiation of γ-ATP (−2.48 pm) were compared and plotted by varying the number of frequency selective Gaussian pulses of 100 ms each. We used 10, 20, 30 and 40 pulses with an interpulse delay of 200 μs. We also varied the power of the pulse by increasing its nominal flip angle from 90°, 180°, 360° and 720°, while remaining within the SAR safety limits.

^{31}P-MRI

PCr Imaging with 3D-TSE—We obtained images using a 3D-TSE sequence (described in our previous work (32)). In our sequence, the 90° excitation pulse is spectrally selective (Gaussian shape with 8 ms duration, and full width at half maximum of 220 Hz) in order to excite only a single resonance of the ^{31}P spectrum (i.e. PCr), and is implemented without the use of a slice selective gradient. The sequence is sampling k-space in a centric manner. A train of 24 echoes (ETL = 24) is sampled along the primary phase encoding direction (in this case, anterior to posterior), with 26 ms echo spacing. Spin echoes are sampled with a 2.5 kHz bandwidth. This k-space sampling scheme results in increased blurring in the imaging direction where the ETL is sampled. We simulated the effect of modulation of signal during the ETL acquisition in order to predict the point-spread-function (PSF) along that direction, using an average T_2 value of PCr of 153 ± 30 ms of the calf muscle that we have measured previously (27) and is in close agreement with T_2 values reported in the literature (33).

It has been shown previously that the signals of the ATP ^{31}P resonances after excitation modulate both in amplitude and phase due to J-coupling among the individual resonances of that molecule (22,25). For the case of multi-echo sequences (such as the TSE employed in this study), ATP signals cancel out when the echo-spacing is set to 26 ms, hence minimizing any contamination of the PCr signal from off-resonance excitation of ATP.

PCr Quantification—In order to quantify the absolute PCr concentration we used a phantom substitution method. In a separate experiment, we scanned a phantom with comparable to the in vivo coil loading, using the same 3D-TSE sequence and acquisition parameters, with the exception of a longer TR (60 s). The phantom was used to derive the calibration curve of PCr as a function of signal intensity. It consisted of two sealed cylindrical tubes containing different inorganic phosphate concentrations (25 and 50 mM). In vivo PCr images were corrected for B_1 inhomogeneities (34,35). Signal intensities of the corrected PCr images were compared voxel-wise to the calibration line obtained from the phantoms to extract PCr concentration maps ([PCr]). These concentrations are in mmol/L of

tissue and can be converted to mmol/L of cell water (mM) by a conversion factor (in this case equal to 1.41) that takes into account the water content of the muscle (36).

T_1' mapping in the muscles of the lower leg—The imaging sequence described above was slightly modified in order to measure T_1' in the muscles of the lower leg. In the inversion recovery 3D-TSE sequence (t-180-TI-imaging), while saturation of the γ-ATP was performed during both time interval,(t), and inversion time, (TI). During time t, the same train of 40 Gaussian pulses described in the previous section was used (100 ms durations, 360° nominal flip angle), while eight images were acquired at different TIs (100, 300, 500, 700, 1500, 3000, 5000, 8000 ms). Inversion was achieved using an adiabatic inversion pulse (WURST shape (37), duration 5 ms, bandwidth 250 Hz). A schematic of the pulse sequence is shown in Fig.1.A. We obtained average T_1' values for each muscle by segmenting the entire volume of each muscle and fitting a single exponential growth function. In addition, we obtained 3D T_1' maps by fitting a single exponential growth function in each voxel.

CK reaction rate and metabolic flux mapping—To map the kinetics of the CK reaction rate in the different muscles of the lower leg, we acquired images using a 3D-TSE sequence with MT preparation (Fig.1B). The MT preparation module comprised of a train of 40 Gaussian pulses, each with 100 ms duration and 360° nominal flip angle, followed by a large crusher gradient (25 ms duration) to destroy any remaining transverse magnetization prior to excitation. We obtained three 3D-imaging data sets, one without irradiation, and a pair of images where the MT preparation was applied on the γ-ATP resonance (−2.48 ppm) and the mirrored side relative to PCr (+2.48 ppm). All the 3D-data sets had field-of-view (FOV) of 220 × 220 × 200 mm, acquisition matrix size of 48 × 48 × 8, yielding nominal resolution of 4.6 × 4.6 × 25 mm^3 (voxel size = 0.52 mL), with TR of 12 s, and scan time of 3 min and 12 s per average, while 3 averages were obtained for each 3D-data set.

We estimated CK reaction rate constants and metabolic fluxes voxel-wise using Eq.1–2, after correcting for T_1'. We also estimated average CK reaction rate constants and metabolic fluxes for each individual muscle by segmenting the entire volume of the muscle and applying Eq.1–2 in the average signal intensity. During the MT imaging experiments, the SAR levels never exceeded 15% of the maximum allowed under normal operating mode.

^{1}H-MRI

To verify muscle anatomy, we used a product gradient echo (GRE) sequence to acquire 3D-^{1}H images (with the same FOV and orientation as the ^{31}P images) in all volunteers. Acquisition parameters were: matrix size: 128 × 128 × 40; TR: 20 ms; TE: 3.5 ms; FA: 8°; acquisition time: 1 min 44 s.

Statistical Analyses

We performed one-way analysis of variance (ANOVA) for the measurements (T_1', k_{CK}, V_{CK}) obtained in individuals muscles of the five healthy subjects. Post hoc analysis was performed using Tukey's Post hoc test. Significance was set at $p < 0.05$ level.

Results

MT pulse train design with unlocalized ^{31}P-MRS

An example of unlocalized ^{31}P-MRS data acquired from the entire volume of muscle of the lower leg of a healthy volunteer can be seen in Fig.2A, using a train of 40 such pulses (yielding a total irradiation time of 4 s). Each pulse has a nominal flip angle of 360° each. In Fig.2A reference MR spectrum (no irradiation), a control (irradiation at +2.48 ppm), and a

spectrum where the γ-ATP resonance is irradiated (−2.48 ppm), are shown from a healthy volunteer. We varied the number of pulses from 10 to 40 (hence the irradiation time from 1 to 4 s), and the power of the pulses (from 90° to 720°), while remaining within the SAR safety limits. The results are shown in Fig.2B. Based on these results we chose to use a train of 40 Gaussian pulses with 360° nominal flip angle each, although increased power (i.e. 720°) resulted in slightly higher MT contrast, due to the significantly increased duty cycle of the latter.

Simulation of the PSF

We simulated the PSF of our imaging sequence, using T_2 relaxation parameters of the calf muscle measured previously (27). By simulating the effect of modulation of signal during the ETL acquisition we estimated the PSF at 2.8 pixels in the imaging direction that the ETL is sampled (anterior to posterior). A visualization of the simulated blurring results is shown in Fig.3.

T_1' mapping in different muscles of the lower leg

We measured T_1' in several muscles of the lower leg while saturating the γ-ATP resonance. Images acquired at different TIs can be seen in Fig.4A. The anatomy of the muscles from the proton image is shown in Fig.4B, and an example of fitting of the data from the tibialis anterior (TA) muscle is shown in Fig.4C. By using this technique we had the required spatial resolution to measure T_1' in the different muscles of the lower leg in five healthy volunteers. The results are summarized in Table 1. No statistically significant differences were observed among the T_1' values of the different muscles of the healthy subjects.

CK reaction rate and metabolic flux mapping

An example of 3D-images using a 3D-TSE sequence with MT preparation is shown in Fig.5. Figure 5A shows the anatomical ^{1}H slices, Fig.5B shows the control ^{31}P imaging experiment, while Fig.5C shows the images acquired when the γ-ATP was irradiated. Using Eq.1, the CK reaction rate was measured after correcting for T_1' (Fig.5D). The results for all healthy volunteers are summarized in Table 2. The metabolic fluxes for the different muscles for each subject are shown in Table 3. The map of metabolic fluxes can be seen in Fig.5D. In the group of the five healthy volunteers, the reaction rate constants between TA and GL muscles were statistically different ($p = 0.0324$), as well as the metabolic fluxes between these two muscles ($p = 0.0426$).

Detection of muscle energy abnormalities in diabetic patients

The same experimental protocol was implemented on two clinically diagnosed type 2-diabetic patients, and in both cases we observed spatial variation of the CK reaction rate. In Fig.6, the ^{1}H anatomical images (Fig.6A), the control and MT ^{31}P imaging experiments (Fig.6B–C), the CK reaction rate map (Fig.6D), and the metabolic flux maps (Fig.6D) can be seen of a 48 year-old patient. As shown in Fig.6D, there is an area in the gastrocnemius medial (GM), where the CK reaction rate is significantly lower ($k_{CK} = 0.18\ s^{-1}$, which is nine standard deviations lower), compared to the healthy subjects. The rest of the muscles of the lower leg the reaction rate is within the limits of the healthy volunteers ($0.22 – 0.25\ s^{-1}$), likely due to a disease-specific feature of the diabetic muscle. The second diabetic patient, also showed reduced CK reaction rate kinetics in the GM ($k_{CK} = 0.20\ s^{-1}$, which is seven standard deviations lower), compared to the healthy subjects.

Discussion

The results presented in this work, demonstrate that quantitative mapping of the kinetics of an important metabolic reaction (i.e. [CK]) can be achieved in the entire volume of the calf muscle at relatively high spatial resolution (0.52 mL voxel size), with reasonable acquisition time that can be tolerated by patients (below 60 min), using spectrally selective imaging sequence. This is important because very little is known about the spatial localization of metabolic properties in either healthy or diseased states. Having a tool to study those spatial heterogeneities can improve our understanding of patterns of disease presentation and progression, and will allow us to longitudinally track the effectiveness of therapeutic interventions.

To the best of our knowledge, only one study has performed MT measurements in skeletal muscle at 7T. Valkovic et al. (38), reported unlocalized MRS measurement in the gastrocnemius of healthy volunteers with average T_1' of PCr of 1.54 s. The average measured T_1' with our method in the gastrocnemius lateral (GL) was 1.79 s, and 1.82 s in the gastrocnemius medial (GM). In that same study Valkovic and colleagues measured the CK reaction rate constant at 0.34 s^{-1}. Our measured k_{CK} were on average 0.29 s^{-1} and 0.27 s^{-1} in the GL and GM respectively. Bottomley et al. (19), performed measurements at 1.5T in the calf muscle and measured the CK reaction rate at 0.29 s^{-1} using unlocalized MRS, and 0.27 s^{-1} using a localized experiment, which is in very close agreement with our measurement. Metabolic fluxes measured with MRS methods, usually are calculated under the assumption that the concentration of γ-ATP is constant at 8.2 mM, and PCr concentration is inferred by comparing the relative area under the two peaks (36). Under this assumption, Valkovic et al (38), measured the metabolic fluxes in the gastrocnemius at 7.58 mM s^{-1}. As seen in Table 3, our measured metabolic fluxes in healthy controls were on average 8.91 mM s^{-1} and 8.42 mM s^{-1} for the GL and GM respectively. In the case of the diabetic patients, our method detected decreased CK rate in the GM, while the CK reaction rates in the rest of the muscles of the lower leg were within the range of the healthy volunteers. This result, although in need of replication, suggests that spatial mapping of metabolic turnover rates may identify regions of skeletal muscle affected by pathology that have remained undetected with single voxel acquisitions. Not all muscle bundles are the same, some may be slow twitch (red muscle), which are rich in capillaries and mitochondria and myoglobin (39). Slow twitch muscle generates its energy aerobically from fats and carbohydrates and can sustain long-term contraction, but are not very powerful. Fast twitch (white muscle), has less capillaries and mitochondria, and contracts more rapidly and powerfully but because it uses predominantly anaerobic metabolism, it is far less efficient in ATP generation and tires more easily because of lactate production (40). These major differences in energetic flux can be distinguished by our high spatial resolution method and would allow us to ascertain whether diabetes affect different muscles that may have different proportions of fast and slow twitch fibers.

It is well documented that skeletal muscle has a high degree of organization at different spatial levels. This order has several distinct effects on in vivo MR that have been observed, especially in ^{1}H spectra. In particular, dipolar coupling effects due to anisotropic motional averaging have been shown for the ^{1}H resonances of creatine, taurine and lactate (41). Quantification of lipids (i.e. intramyocellular and extramyocellular) is affected by bulk magnetization susceptibility effects and is also strongly dependent on the orientation under which they are measured (42,43). However, similar orientation dependent effects have not been reported for either PCr or ATP.

Magnetization Transfer imaging studies, either spectroscopic or spectrally selective in the skeletal muscle, have not, to the best of our knowledge, been reported previously.

Magnetization Transfer studies utilizing large voxel sizes (between 6 and 8 mL) have been previously reported in brain (17,18) at 7T. Our method yields nominal voxel sizes of 0.52 mL, however any comparison between studies in skeletal muscles and brain need to take into account the large difference in PCr concentration between the two types of tissue (brain: ~ 3mM (44,45) and skeletal muscle: ~ 30 mM (36)). Therefore, we believe that our method could be used for brain, although given the lower PCr concentration likely at lower spatial resolution than what is possible in skeletal muscle. Another potential application of our sequence would be to map CK kinetics in heart, where currently only single voxel MRS methods have been utilized (46). At lower resolution (nominal voxel size = 1.6 mL) we have shown that we are able to acquire 3D volumetric data in 24s acquisition time with full k-space sampling (29), or 12s using Compressed Sensing ^{31}P-MRI (28). These acquisition times are on the same order as 31P-MRS methods that have been used for cardiac studies (20).

Another key reaction in energy metabolism that has been studied with ^{31}P-MRS is the synthesis of ATP through chemical exchange with Pi (ATPase) (2). With our method, this reaction could potentially be studied with a separate set of experiments, including T_1' measurements of Pi. Recently, two metabolites have been measured during spectrally selective imaging acquisitions, either using interleaved excitation (47), or simultaneous excitation of the two metabolites using dual-band RF pulses (48,49) and could be used for measuring both reaction rates (i.e. CK and ATPase) more time efficiently.

This study was performed at ultra high field strength (7T), which compared to high-field strength clinical magnets (3T) delivers 2.5 to 3.0 fold increased SNR in ^{31}P experiments (50,27,38). We have shown previously that PCr concentration mapping can be performed at 3T (32) with our method. Therefore, the MT-imaging method presented here could potentially be implemented at lower field, albeit at the cost of longer acquisition time or lower spatial resolution.

We have measured a mean T_2 value of 153 ± 30 ms at 7T, using the average value, the anterior to posterior PSF was measured at 2.8 pixels. Broadening of the PSF in the anterior-to-posterior direction can have an effect on our ability to segment accurately individual muscles. The voxels at the interface of the muscles will contain signals from more than one muscle. Therefore, voxels away from the boundaries of the muscle are more likely to depict the properties of the muscle. On the other hand, imperfections of the 180° pulses result in stimulated echoes that increase the apparent T_2, hence reduce the blurring effect (21). For the current study these effects have not been included in the estimation of the PSF, however it would be worth investigating in future studies. There are known methods in the literature for splitting the blurring effect and distributing it into more than one imaging dimensions that simply require re-programming of the phase-encoding gradient waveform of our method (51).

In this study, all healthy subjects had BMI < 26. There were no signs of fat infiltration in the muscle in the ^{1}H images. Therefore, we assumed constant water content in all muscles. From the two patients, one had BMI = 26.2 and similarly to the healthy no signs of fat infiltration were observed from the ^{1}H images. For the second patient (BMI = 34.1), quantification of PCr concentration was performed in segmentations of the muscles away from fat containing voxels. In general, obese subjects (BMI > 30) can have higher fat content in the muscle tissue. In addition, many muscle weakening and metabolic disorders lead to an increase in adipose tissue in and around the muscles, which will influence PCr quantification, if not accounted for. Thus, 3D mapping of the absolute PCr concentration in the entire muscle tissue must include a fat/water quantification step in order to estimate the

actual PCr concentration.. Currently, there are several fat/water separation methods reported in the literature (52,53) that we will explore in the future.

In summary, the results of this work have shown that 3D-mapping of the CK forward reaction rates and metabolic fluxes can be achieved in skeletal muscle at relatively high spatial resolution, within experimental times that can be tolerated by patients. Having the ability to study this important enzymatic reaction in large areas of the muscles can bring new insights into differential localization and patterns of muscle bioenergetics caused by several diseases and can become a valuable tool for monitoring the progression of disease or the efficacy of interventions.

Acknowledgments

Grant sponsor: The authors would like to acknowledge the support by research grants RO1 AR053133, RO1 AR056260, and RO1 AR060238 from the National Institute of Arthritis and Musculoskeletal and Skin Diseases (NIAMS), National Institutes of Health (NIH).

LIST OF ABBREVIATIONS

ADP	Adenosine diphosphate
ATP	Adenosine triphosphate
CK	Creatine kinase
CW	Continuous wave
GL	Gastrocnemius lateral muscle
GM	Gastrocnemius medial muscle
MT	Magnetization transfer
P	Peroneus muscle
PCr	Phosphocreatine
Pi	Inorganic phosphate
R	Pearson's correlation
S	Soleus muscle
SD	Standard deviation
$\mathbf{T_1'}$	Spin lattice relaxation when γ-ATP is saturated
TA	Tibialis anterior muscle
TI	Inversion time
TP	Tibialis posterior muscle
TSE	Turbo spin echo

References

1. Kemp GJ, Radda GK. Quantitative interpretation of bioenergetic data from 31P and 1H magnetic resonance spectroscopic studies of skeletal muscle. Magn Reson Q. 1994; 10(1):43–63. [PubMed: 8161485]
2. Alger JR, Shulman RG. NMR-studies of enzymatic rates in vitro and in vivo by magnetization transfer. Q Rev Biophys. 1984; 17(1):83–124. [PubMed: 6091170]

3. Moller HE, Wiedermann D. Magnetization-transfer P-31 NMR of biochemical exchange in vivo: Application to creatine kinase kinetics. Journal of Spectroscopy. 2002; 16(3–4):207–216.
4. Jennings RB, Reimer KA. Lethal myocardial ischemic-injury. Am J Pathol. 1981; 102(2):241–255. [PubMed: 7008621]
5. Ingwall JS. Is cardiac-failute a consequence of decreased energy reserve? Circulation. 1993; 87(6): 58–62.
6. Radda GK. The use of NMR spectroscopy for the understanding of disease. Science. 1986; 233(4764):640–645. [PubMed: 3726553]
7. Duncan BB, Schmidt MI, Pankow JS, Ballantyne CM, Couper D, Vigo A, Hoogeveen R, Folsom AR, Heiss G. Low-grade systemic inflammation and the development of type 2 diabetes - The atherosclerosis risk in communities study. Diabetes. 2003; 52(7):1799–1805. [PubMed: 12829649]
8. Kelley DE, He J, Menshikova EV, Ritov VB. Dysfunction of mitochondria in human skeletal muscle in type 2 diabetes. Diabetes. 2002; 51(10):2944–2950. [PubMed: 12351431]
9. Befroy DE, Shulman GI. Magnetic Resonance Spectroscopy Studies of Human Metabolism. Diabetes. 2011; 60(5):1361–1369. [PubMed: 21525507]
10. Hands LJ, Bore PJ, Galloway G, Morris PJ, Radda GK. Muscle metabolism in patients with peripheral vascular-disease investigated by 31P nuclear-magnetic resonance spectroscopy. Clin Sci. 1986; 71(3):283–290. [PubMed: 3757432]
11. Prompers JJ, Jeneson JAL, Drost MR, Oomens CCW, Strijkers GJ, Nicolay K. Dynamic MRS and MRI of skeletal muscle function and biomechanics. NMR Biomed. 2006; 19(7):927–953. [PubMed: 17075956]
12. Taylor DJ. Clinical utility of muscle MR spectroscopy. Seminars in musculoskeletal radiology. 2000; 4(4):481–502. [PubMed: 11371330]
13. Lanza IR, Larsen RG, Kent-Braun JA. Effects of old age on human skeletal muscle energetics during fatiguing contractions with and without blood flow. J Physiol (Lond). 2007; 583(3):1093–1105. [PubMed: 17673506]
14. Oberbach A, Bossenz Y, Lehmann S, Niebauer J, Adams V, Paschke R, Schon MR, Bluher M, Punkt K. Altered fiber distribution and fiber-specific glycolytic and oxidative enzyme activity in skeletal muscle of patients with type 2 diabetes. Diabetes Care. 2006; 29(4):895–900. [PubMed: 16567834]
15. Parry A, Matthews PM. Roles for imaging in understanding the pathophysiology, clinical evaluation, and management of patients with mitochondrial disease. J Neuroimaging. 2003; 13(4): 293–302. [PubMed: 14569820]
16. Bottomley PA, Ouwerkerk R. Optimum flip-angles for exciting NMR uncertain T1 values. Magn Reson Med. 1994; 32(1):137–141. [PubMed: 8084230]
17. Fei D, Xiao-Hong Z, Hongyan Q, Xiaoliang Z, Wei C. Efficient in vivo 31P magnetization transfer approach for noninvasively determining multiple kinetic parameters and metabolic fluxes of ATP metabolism in the human brain. Magn Reson Med. 2007; 57(1)
18. Pan, JW.; Avdievich, N.; Spencer, D.; Hetherington, HP. 31P Exchange Sensitive Imaging in Human Brain at 7T. Proc Seventeenth Meeting Proceedings (ISMRM, Honolulu, Hawaii); 2009; Honolulu, Hawai.
19. Bottomley PA, Ouwerkerk R, Lee RF, Weiss RG. Four-angle saturation transfer (FAST) method for measuring creatine kinase reaction rates in vivo. Magn Reson Med. 2002; 47(5):850–863. [PubMed: 11979563]
20. Schar M, El-Sharkawy A-MM, Weiss RG, Bottomley PA. Triple Repetition Time Saturation Transfer (TRiST) (31)P Spectroscopy for Measuring Human Creatine Kinase Reaction Kinetics. Magn Reson Med. 2010; 63(6):1493–1501. [PubMed: 20512852]
21. Chao H, Bowers JL, Holtzman D, Mulkern RV. RARE imaging of PCr in human forearm muscles. J Magn Reson Im. 1997; 7(6):1048–1055.
22. Chao H, Bowers JL, Holtzman D, Mulkern RV. Multi-echo 31P spectroscopic imaging of ATP: A scan time reduction strategy. J Magn Reson Im. 1997; 7(2):425–433.
23. Greenman RL, Elliott MA, Vandenborne K, Schnall MD, Lenkinski RE. Fast imaging of phosphocreatine using a RARE pulse sequence. Magn Reson Med. 1998; 39(5):851–854. [PubMed: 9581617]

24. Greenman RL, Axel L, Ferrari VA, Lenkinski RE. Fast imaging of phosphocreatine in the normal human myocardium using a three-dimensional RARE pulse sequence at 4 tesla. J Magn Reson Im. 2002; 15(4):467–472.
25. Greenman RL. Quantification of the P-31 metabolite concentration in human skeletal muscle from RARE image intensity. Magn Reson Med. 2004; 52(5):1036–1042. [PubMed: 15508151]
26. Greenman RL, Smithline HA. The feasibility of measuring phosphocreatine recovery kinetics in muscle using a single-shot (31)P RARE MRI sequence. Acad Radiol. 2011; 18(7):917–923. [PubMed: 21536463]
27. Parasoglou, P.; Xia, D.; Chang, G.; Regatte, RR. Spectrally selective 3D imaging of phosphocreatine in the human calf muscle at 3T and 7T. Proc Twentieth Meeting Proceedings (ISMRM, Melbourne, Australia); 2012; Melbourne, Australia.
28. Parasoglou P, Feng L, Xia D, Otazo R, Regatte RR. Rapid 3D-Imaging of Phosphocreatine Recovery Kinetics in the Human Lower Leg Muscles with Compressed Sensing. Magn Reson Med. 2012; 68(6):1738–1746. [PubMed: 23023624]
29. Parasoglou P, Xia D, Chang G, Regatte RR. Dynamic Imaging of Phosphocreatine Recovery Kinetics in the Human Lower Leg Muscles at 3T and 7T: A preliminary Study. NMR Biomed. 201210.1002/nbm.2866
30. Forsen S, Hoffman RA. Study of moderately rapid chemical exchange reactions by means of nuclear magnetic double resonance. J Chem Phys. 1963; 39(11):2892.
31. Sun PZ, Benner T, Kumar A, Sorensen AG. Investigation of optimizing and translating pH-sensitive pulsed-chemical exchange saturation transfer (CEST) imaging to a 3T clinical scanner. Magn Reson Med. 2008; 60(4):834–841. [PubMed: 18816867]
32. Parasoglou P, Xia D, Regatte RR. Spectrally selective 3D TSE imaging of phosphocreatine in the human calf muscle at 3 T. Magn Reson Med. 201210.1002/mrm.24288
33. Bogner W, Chmelik M, Schmid AI, Moser E, Trattnig S, Gruber S. Assessment of (31)P Relaxation Times in the Human Calf Muscle: A Comparison between 3 T and 7 T In Vivo. Magn Reson Med. 2009; 62(3):574–582. [PubMed: 19526487]
34. Collewet G, Davenel A, Toussaint C, Akoka S. Correction of intensity nonuniformity in spin-echo T(1)-weighted images. Magn Reson Imaging. 2002; 20(4):365–373. [PubMed: 12165356]
35. Yarnykh VL. Actual flip-angle imaging in the pulsed steady state: A method for rapid three-dimensional mapping of the transmitted radiofrequency field. Magn Reson Med. 2007; 57(1):192–200. [PubMed: 17191242]
36. Kemp GJ, Meyerspeer M, Moser E. Absolute quantification of phosphorus metabolite concentrations in human muscle in vivo by P-31 MRS: a quantitative review. NMR Biomed. 2007; 20(6):555–565. [PubMed: 17628042]
37. Kupce E, Freeman R. Adiabatic pulses for wide-band inversion and broadband decoupling. J Magn Reson Ser A. 1995; 115(2):273–276.
38. Valkovic L, Chmelik M, Kukurova IJ, Krssak M, Gruber S, Frollo I, Trattnig S, Bogner W. Time-resolved phosphorous magnetization transfer of the human calf muscle at 3 T and 7 T: A feasibility study. Eur J Radiol. 10.1016/j.ejrad.2011.09.024
39. Johnson MA, Polgar J, Weightma D, Appleton D. Data on distribution of fiber types in 36 human muscles. Autopsy study J Neurol Sci. 1973; 18(1):111–129.
40. Hood DA. Plasticity in skeletal, cardiac, and smooth muscle - Invited review: Contractile activity-induced mitochondrial biogenesis in skeletal muscle. J Appl Physiol. 2001; 90(3):1137–1157. [PubMed: 11181630]
41. Boesch C, Kreis R. Dipolar coupling and ordering effects observed in magnetic resonance spectra of skeletal muscle. NMR Biomed. 2001; 14(2):140–148. [PubMed: 11320539]
42. Boesch C, Machann J, Vermathen P, Schick F. Role of proton MR for the study of muscle lipid metabolism. NMR Biomed. 2006; 19(7):968–988. [PubMed: 17075965]
43. Marjanska M, Eberly LE, Adriany G, Verdoliva SN, Garwood M, Chow L. Influence of foot orientation on the appearance and quantification of (1) H magnetic resonance muscle spectra obtained from the soleus and the vastus lateralis. Magn Reson Med. 2012; 68(6):1731–1737. [PubMed: 22298295]

44. Hetherington HP, Spencer DD, Vaughan JT, Pan JW. Quantitative P-31 spectroscopic imaging of human brain at 4 tesla: Assessment of gray and white matter differences of phosphocreatine and ATP. Magn Reson Med. 2001; 45(1):46–52. [PubMed: 11146485]
45. Du F, Zhu X-H, Qiao H, Zhang X, Chen W. Efficient in vivo P-31 magnetization transfer approach for noninvasively determining multiple kinetic parameters and metabolic fluxes of ATP metabolism in the human brain. Magn Reson Med. 2007; 57(1):103–114. [PubMed: 17191226]
46. Degani H, Laughlin M, Campbell S, Shulman RG. Kinetics of creatine kinase in heart- A P31 saturation-transfer and inversion-transfer study. Biochemistry. 1985; 24(20):5510–5516. [PubMed: 4074712]
47. Greenman RL, Wang X, Smithline HA. Simultaneous acquisition of phosphocreatine and inorganic phosphate images for Pi:PCr ratio mapping using a RARE sequence with chemically selective interleaving. Magn Reson Imaging. 2011; 29(8):1138–1144. [PubMed: 21641744]
48. Steinseifer, IK.; Wijnen, JP.; Hamans, BC.; Heerschap, A.; TWS. Fast 31P metabolic imaging of human muscle. Proc Eighteenth Meeting Proceedings (ISMRM, Sotckholm, Sweden); Stockholm, Sweden.
49. Lu A, Atkinson IC, Zhou XJ, Thulborn KR. PCr/ATP ratio mapping of the human head by simultaneously imaging of multiple spectral Peaks with interleaved excitations and flexible twisted projection imaging readout trajectories at 9.4 T. Magn Reson Med. 201210.1002/mrm.24281
50. Bogner W, Chmelik M, Andronesi OC, Sorensen AG, Trattnig S, Gruber S. In Vivo (31)P Spectroscopy by Fully Adiabatic Extended Image Selected In Vivo Spectroscopy: A Comparison Between 3 T and 7 T. Magn Reson Med. 2011; 66(4):923–930. [PubMed: 21446033]
51. Kholmovski EG, Parker DL, Alexander AL. A generalized k-sampling scheme for 3D fast spin echo. J Magn Reson Im. 2000; 11(5):549–558.
52. Reeder SB, McKenzie CA, Pineda AR, Yu H, Shimakawa A, Brau AC, Hargreaves BA, Gold GE, Brittain JH. Water-fat separation with IDEAL gradient-echo imaging. J Magn Reson Imag. 2007; 25(3):644–652.
53. Karampinos DC, Baum T, Nardo L, Alizai H, Yu H, Carballido-Gamio J, Yap P, Shimakawa A, Link TM, Majumdar S. Characterization of the regional distribution of skeletal muscle adipose tissue in type 2 diabetes using chemical shift-based water/fat separation. J Magn Reson Imag. 2012; 35(4):899–907.

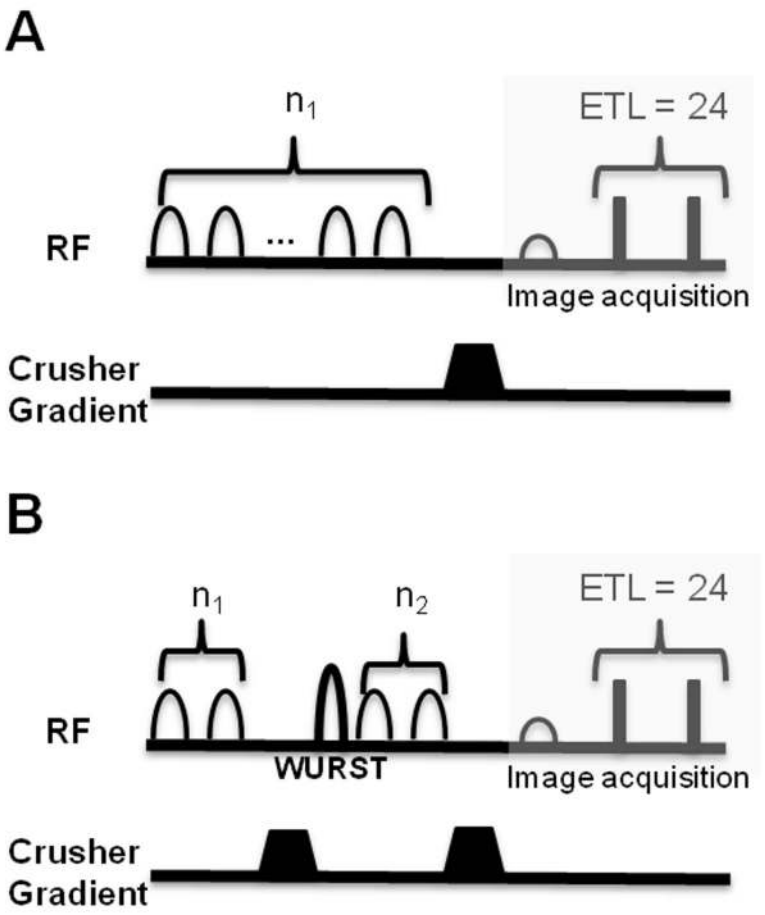

Fig. 1.

MT and T_1' ^{31}P-Imaging pulse sequences. A) T_1' measurement while suppressing the γ-ATP peak with a train of 40 Gaussian pulses of 100 ms duration each and 360° nominal flip angle applied during n_1. Inversion of the PCr peak is achieved with the use of an adiabatic WURST pulse (5 ms duration, 250 Hz bandwidth). Irradiation of γ-ATP is also performed during the inversion time, by varying the number of pulses used in n_2. Image acquisition is performed with a 3D-TSE sequence. B) The MT preparation module comprised of a train of 40 Gaussian pulses, each with 100 ms duration and 360° nominal flip angle applied either on the γ-ATP peak or the mirror side relative to PCr (control experiment), followed by a 3D-TSE imaging acquisition.

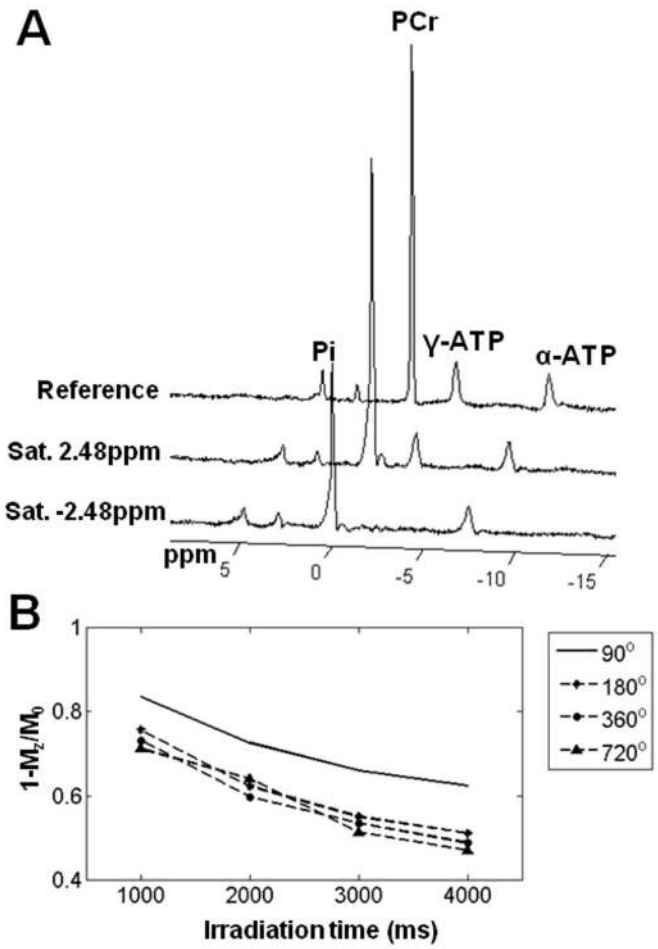

Fig. 2.

MT pulse train design with ^{31}P MRS. A) Sample spectra of magnetization transfer experiment in the human calf muscle. A reference spectrum collected without suppression, a control spectrum with suppression frequency at +2.48 ppm relative to PCr, and a spectrum acquired with suppression of the γ-ATP peak. An MT train of 40 Gaussian pulses (each 100 ms long, with nominal flip angle of 360°) was used for the suppression. B) MT contrast pulse optimization. We compared the contrast introduced by the train of MT pulses using unlocalized ^{31}P-MRS in the entire volume of the lower leg. We varied the irradiation time, as defined by the number of 100 ms Gaussian pulses (from 10 to 40 pulses, yielding irradiation times of 1 to 4 s), and the power defined by the nominal flip angle of each pulse (from 90° to 720°). We decided to use 40 pulses with 360° nominal flip angle, which produced 45 % contrast (M_z/M_0), while remaining within the safety SAR limits.

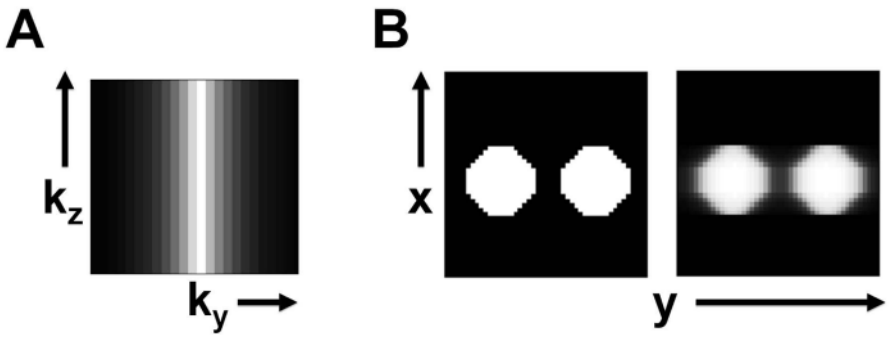

Fig. 3.
Simulation of the PSF induced by the sampling pattern of the 3D-TSE. A) k-space signal modulation resulting from the implemented centric 3D-TSE sampling scheme. B) Blurring effect on a simulated phantom with T_2 = 153 ms (equal to the mean T_2 in the calf muscle measured in healthy volunteers). We estimated the PSF in the y-direction at 2.8 pixels.

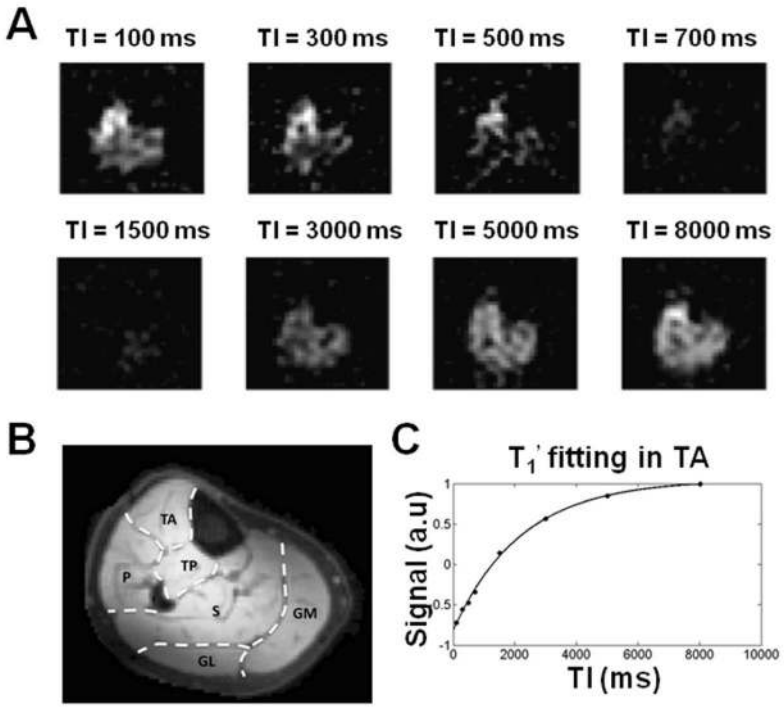

Fig. 4.

T_1' mapping in the muscles of the lower leg. A) Sample images of a cross-section of the muscle at different inversion times. B) Anatomical ^1H image, where the different muscle have been identified. C) Sample measurement of T_1' in the TA in one volunteer. Abbreviations: tibialis anterior (TA), tibialis posterior (TP), peroneus (P), soleus (S), gastrocnemius lateral (GL) and gastrocnemius medial (GM).

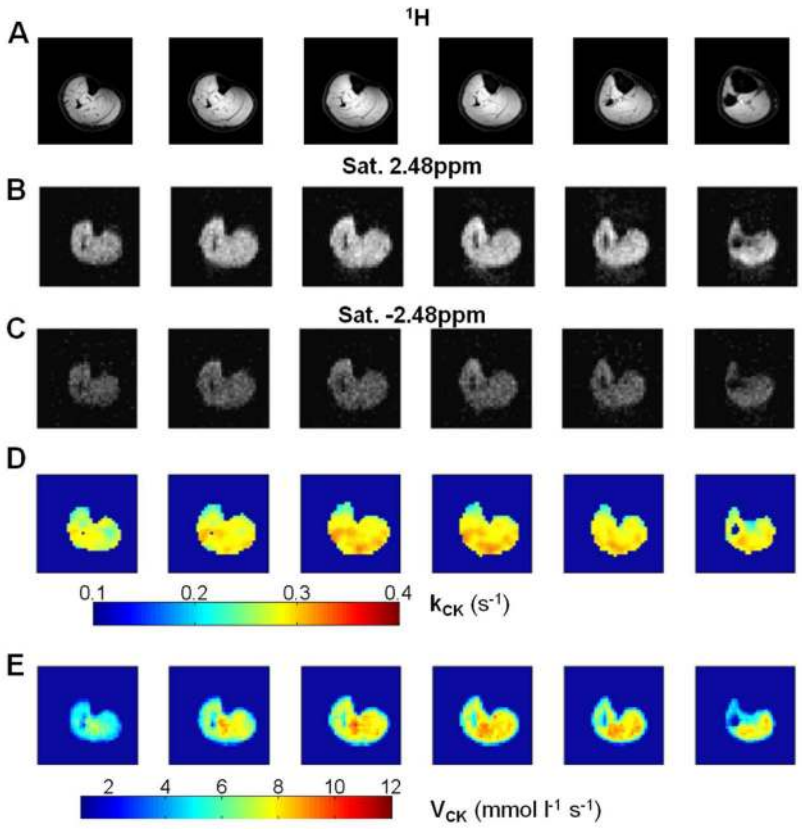

Fig. 5.

Mapping of the kinetic rate (k_{CK}) of the enzymatic creatine kinase reaction rate in the muscles of the lower leg for one healthy volunteer. A) Anatomical ^{1}H slices. B) Control image acquired with the MT preparation module applied at +2.48 ppm. C) Image acquired with the MT pulse train applied on the γ-ATP peak (−2.48 ppm). D) CK reaction rate kinetic mapping in the muscle of the lower leg produced by the ratio of images in B) and C) according to Eq.1 using T_1' measured in a separate experiment E) Spatial mapping of metabolic fluxes.

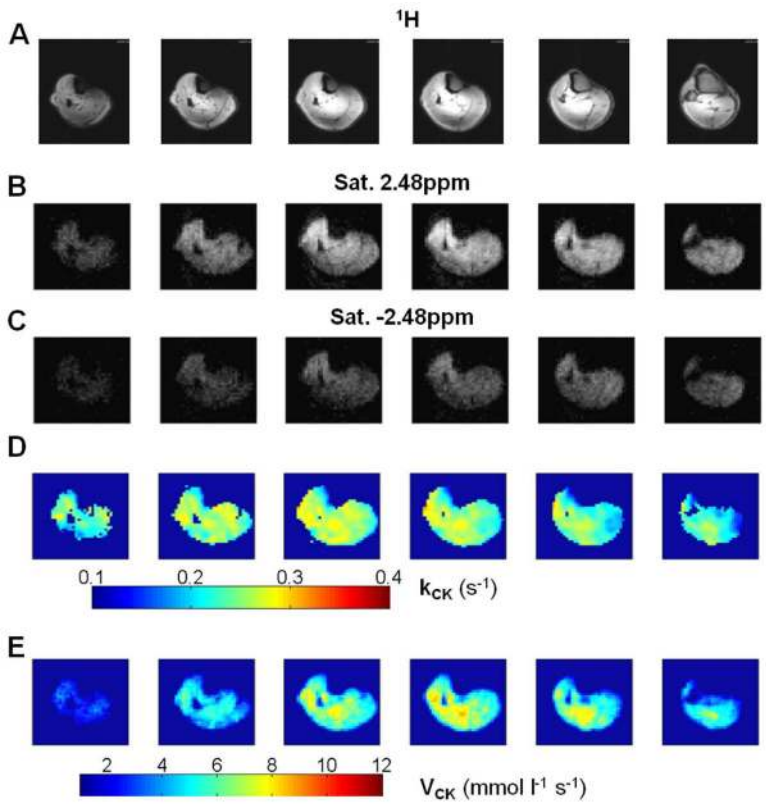

Fig. 6.

Detection of muscle energy abnormalities in the GM muscle of a 48 year-old diabetic patient. A) Anatomical ^{1}H slices. B) Control image acquired with the MT preparation module applied at +2.48 ppm. C) Image acquired with the MT pulse train applied on the γ-ATP peak (−2.48 ppm). D) Lower CK reaction rate (0.18 s^{-1}) was observed in the part of the diabetic leg (GM), likely due to disease specific feature of the diabetic muscle. E) Corresponding metabolic fluxes.

Table 1

Spin-lattice relaxation times T_1' (s) for each healthy subject measured in different muscles of the lower leg. Abbreviations: tibialis anterior (TA), tibialis posterior (TP), peroneus (P), soleus (S), gastrocnemius lateral (GL) and gastrocnemius medial (GM).

Vol	TA	TP	S	P	GL	GM
1	2.10	1.77	1.94	1.85	1.82	1.82
2	1.84	1.95	1.75	1.60	1.76	1.81
3	1.74	1.71	1.75	2.08	1.71	1.78
4	2.19	2.06	1.79	1.89	1.82	1.82
5	2.12	1.83	1.96	1.83	1.86	1.88
Mean (±SD)	2.00 ± 0.20	1.87 ± 0.14	1.84 ± 0.10	1.85 ± 0.17	1.79 ± 0.06	1.82 ± 0.04

Table 2

CK forward reaction rate constants k_{CK} (s^{-1}) in different muscles of the lower leg of healthy subjects

Vol	TA	TP	S	P	GL	GM
1	0.20	0.26	0.27	0.22	0.27	0.27
2	0.24	0.25	0.25	0.33	0.30	0.28
3	0.27	0.29	0.30	0.25	0.30	0.28
4	0.21	0.22	0.28	0.27	0.29	0.27
5	0.21	0.26	0.24	0.25	0.27	0.25
Mean (±SD)	0.23±0.03	0.26±0.02	0.27±0.02	0.26 ± 0.04	0.29±0.02	0.27±0.01

Table 3

Metabolic fluxes V_{CK} (mM s^{-1}) in different muscles of the lower leg of healthy subjects

Vol	TA	TP	S	P	GL	GM
1	6.53	8.17	7.79	6.87	8.42	8.40
2	7.79	7.70	7.59	10.10	9.36	8.83
3	8.28	8.87	8.48	7.62	9.17	8.83
4	6.89	6.81	8.31	8.06	9.11	8.41
5	6.79	8.11	6.77	7.54	8.51	7.65
Mean (±SD)	7.25±0.74	7.93±0.76	7.78±0.67	8.03±1.23	8.91±0.42	8.42±0.48